Chapter 2

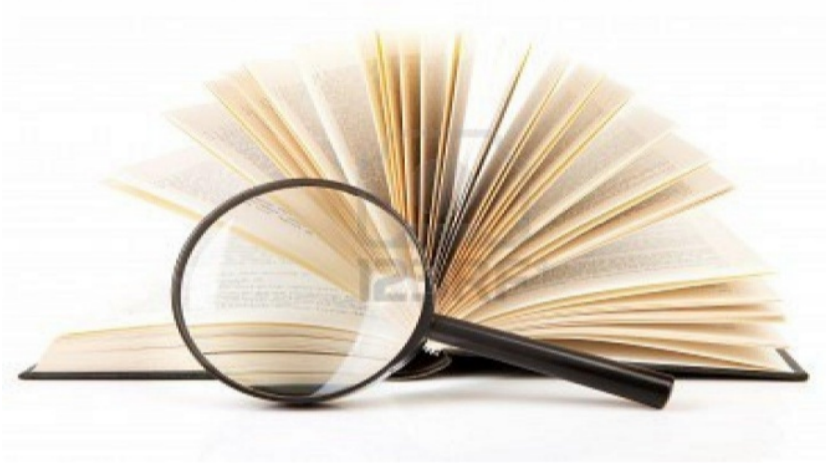

Literature Review

Zinc Oxide, Doping process, ZnO - Bi_2O_3 based Varistor, ZnO -V_2O_5- based Varistor, Impedance spectroscopy studies.

CHAPTER 2

LITERATURE REVIEW

2.1. Zinc Oxide (ZnO): An Overview

Research works on ZnO material started in early 1920s with the first utilization of ZnO for its semiconducting properties as a detector in build-your-own radio sets, in which a thin copper wire, known as "cat's whisker", is placed in contact to sensitive spots on a ZnO crystal [Jagadish et al. (2006)]. ZnO is II-VI inorganic compound semiconductor; exhibiting a wurtzite structure with hexagonal unit cell. ZnO exhibit a wide bandgap semiconductor with large exciton binding energy of 60 meV. It has emerged as a potential candidate in the field of research from the past to till date. The wide direct bandgap transition exhibited by ZnO is much advantageous over indirect bandgap semiconductor as they do not involve phonon transition for wave vector conservation. The wide optical bandgap has a major influence on physical properties of the material like optical absorption, index of refraction, band structure, electrical conductivity and also makes ZnO an efficient emitter and high transparency in the short wavelength applications from blue to UV spectral range. This property enables ZnO to fabricate LED's of various colours (green, blue, red and white), UV photodetectors, UV blue laser diodes, flat panel displays, optical waveguides, transparent electrodes, transistors, nano-generators, solar cells and many more. ZnO materials are subject of intense research as they are low cost, efficient and environment friendly semiconductor material with wide application in gas sensing, catalysis, energy storage, optoelectronic devices, UV lasing action, surface acoustic wave devices, PZT transducers, blue LEDs, TCO, and many more. [Wang et al. (2009); Mende et al. (2007) and Baruah et al. (2009)].

2.1.1. Crystal Structure of Zinc Oxide

At ambient pressure and temperature, ZnO crystallizes to form wurtzite structure which is considered to be the thermodynamically stable phase of ZnO. Wurtzite ZnO is a hexagonal lattice, belonging to the space group of $P6_3mc$ with lattice parameters a = b = 0.3296 nm and c = 0.52065 nm. In an ideal wurtzite crystal, the axial ratio *c/a* and the *u* parameter (which is a measure of the amount by which each atom is displaced with respect to the next along the *c*-axis) are correlated by the relationship $uc/a = (3/8)^{1/2}$ where $c/a = (8/3)^{3/2}$ and $u = 3/8$. The structure of ZnO can be simply described as a number of alternating planes composed of tetrahedrally coordinated O^{2-} and Zn^{2+} ions, stacked alternatively along the *c*-axis. The tetrahedral coordination in ZnO results in non-central symmetric structure and consequently piezoelectric and pyro-electric properties. Additional to the wurtzite phase, ZnO is also known to crystallize in the cubic zinc blende and rocksalt (NaCl) structures, which are illustrated in Figure 2.1 [Özgür et al. (2005)]. Zinc blende (ZnO) is stable only by growth on cubic structures, while the rocksalt structure is a high-pressure metastable phase forming at ~10 GPa, and cannot be epitaxially stabilized. Theoretical calculations indicate that a fourth phase, cubic cesium chloride, may be possible at extremely high temperatures.

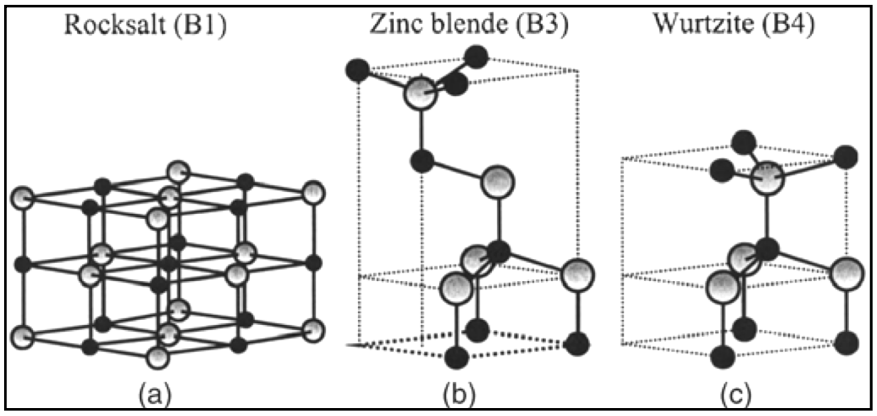

Fig. 2.1: Stick and ball representation of ZnO crystal structures: (a) cubic rocksalt, (b) cubic zinc blende and (c) hexagonal wurtzite structure. The shaded gray and black spheres denote zinc and oxygen atoms respectively [Yogamalar-2013]

2.1.2. Application of Zinc Oxide

ZnO with interesting material properties establishes numerous applications. The world usage of ZnO in 2004 is estimated to be over a million tons. The biggest markets are Asia and Europe (about 300,000 tons ZnO are used in Europe during 2004) [Wenckstern et al. (2009)]. ***ZnO is commercially used as varistor materials***, PZT, sensors, surface acoustic wave devices, TCO (e.g. electrode of ***solar cells***), glasses (reduces thermal expansion coefficient of glasses), rubber industry (effective activator of the curing process of natural rubber, increases heat conductivity in tires, retards de-vulcanization of many rubber types, stabilization of latex foam rubbers, rubber metal bonding), addition to plastics to tune properties like viscosity, fire-resistance, tensile strength, paints, white pigment, phosphors (green phosphors in displays), pharmaceutical industry (antiseptic healing creams, suntan lotions, source of micronutrient zinc), agriculture (addition to fertilizers, source of micronutrient zinc for plants and animals), lubricant (reduce corrosion and wear of engines), photocopying process, anticorrosive coating of metals, constituent of cigarette filters (reducing amounts of HCN and H2S in the smoke). This demonstrates shows the wide use of ZnO in industry.

2.2. Doping Process in Zinc Oxide

Doping of materials is the addition of foreign atoms or impurities purposely. The intention of doping is to modify the physical properties of the materials. For example, pure silicon has poor electrical conducting properties, but it can be doped with boron or arsenic to make it conducting. This opened up a new class of doped-silicon materials, which is now the basis of perhaps the largest global electronics industry. It is well known from present semiconductor technologies that the introduction of impurities or defects into the semiconductor lattices is the primary means of controlling electrical conductivity, optical, luminescent, magnetic, and other electrical properties [Bryan et al. (2005)]. For example, pure stoichiometric ZnO is an insulator; the conductivity of ZnO can be turned over 10

orders of magnitude with the small change in the concentrations of native or non-native defects such as Zn_i or Al dopant. Conventional semiconductor devices, such as the transistor, would not operate without such impurities.

2.2.1. Doping in Zinc Oxide: Intrinsic Defects

The intrinsic or native point defects concerned with ZnO are zinc interstitials Zn_i, oxygen interstitials O_i, zinc vacancies V_{Zn}, oxygen vacancies V_O, zinc antisites Zn_O and oxygen antisites O_{Zn}. In wurtzite ZnO, there exist two different interstitial sites: the tetrahedrally and the octahedrally sites. In ZnO, the octahedrally coordinated interstitials Zn_i and O_i have lower defect formation energies than the tetrahedrally coordinated interstitials Zn_i and O_i. The dominant native donors are the V_O and Zn_i. The ZnO defect in ZnO may also be a relevant donor, although its formation energy is always higher than that of Zn_i. However, it is thermally more stable than Zn_i. So if ZnO is once created by a non-equilibrium process (e.g. irradiation), it is expected to be a relevant donor [Janotti et al. (2009)]. The formation of these donor levels is especially probable, if the fermi energy (FE) is equal to the valence band (V_B) maximum E_V. The $V_O$is a deep donor defect (predicted to be 0.5–1 eV below the conduction band (CB) minimum E_C) and therefore, do not contribute to the free electron concentration. The main native acceptor in ZnO is the V_{Zn}. Its transition level energy is with 0.11 eV above E_V or 0.8 eV above E_V depending on its transition state. The O_i is a deep acceptor defect and its formation energy is higher than that of V_{Zn}. Among the native point defects of ZnO, O_{Zn} has the highest defect formation energy even for oxygen rich conditions and it is considered as a deep acceptor.

At thermal equilibrium, the concentration of point defect is given by the relation [Yogamalar et al. (2013)]

$$c = N_{sites} \exp\left[\frac{-E^f}{k_B T}\right] \tag{2.1}$$

In Eq. (2.1), the N_{sites} is the number of available sites for defect formations, E^f is the defect formation energy, k_B is the Boltzmann constant and T is the absolute temperature in Kelvin.

From the relation it is clear that the defects with high E^f will occur at low concentration. The E^f of the point defects is not constant and it has a greater dependency on synthesis parameters and annealing conditions. Moreover, if the defects are charged then E^f depends on the position of FE. The order of intrinsic defect formation energy E^f in ZnO is $V_{Zn}<V_O<Zn_i<Zn_O<O_i<O_{Zn}$ [Willander et al. (2010)] and the energy levels are represented in Figure 2.2.

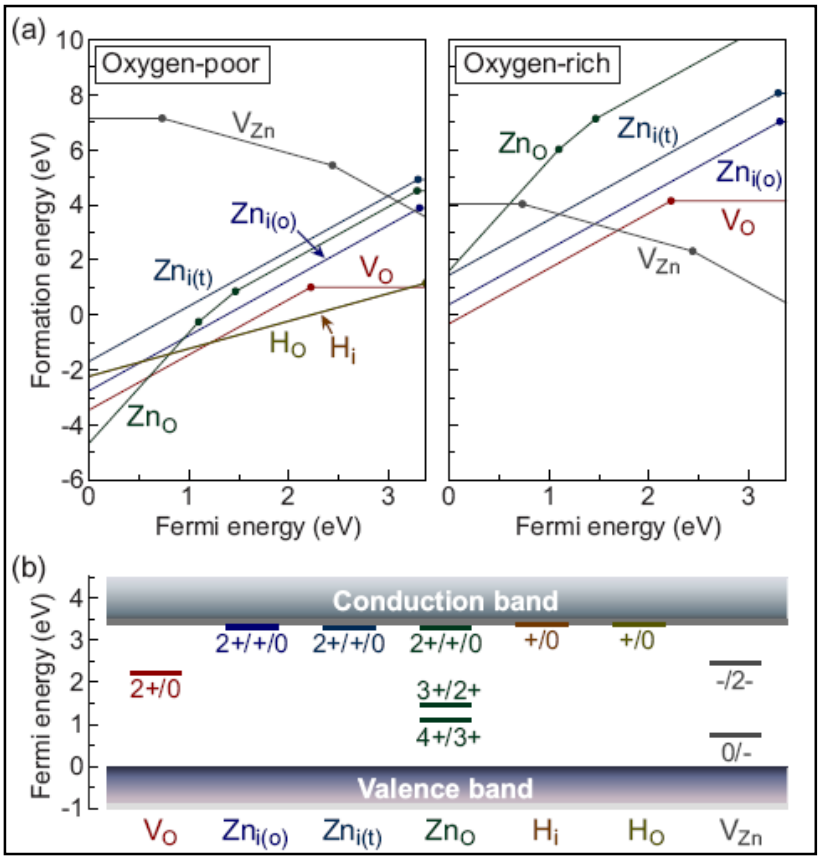

Figure 2.2: (a) Defect formation energies as a function of the FE at the oxygen deficient and oxygen rich limits and (b) Defect thermodynamic transition levels [Yogamalar-2013]

2.2.2. Doping in Zinc Oxide: Extrinsic Defects

N-type ZnO can easily be obtained by doping with Group (III) elements such as Al, Ga, In, transition metal elements such as Pb, Mn, Fe, Ni, Co and rare earth elements like Eu, Y, and Gd. The elements incorporate readily on the zinc lattice site and form shallow ***effective mass donors***. Hydrogen, being an amphoteric defect in many semiconductors, is always a donor in ZnO. It is a shallow defect and can significantly contribute to the free electron concentration of *n*-type ZnO.

The realization of ***p*-type ZnO** for practical applications has ***proven difficult*** and thought to be the bottleneck in the development of ZnO based devices due to the asymmetric doping limitations in ZnO.

2.3. Classical ZnO-Bi_2O_3 based Varistor

In the classical ZnO-based varistor, ***Bi_2O_3 is used as the varistor-former*** [Matsuoka (1969)], thus it is essential for inducing the nonlinearity of the ZnO ceramics [Matsuoka (1971)]. Bi_2O_3 is particularly important since it provides the medium for ***liquid-phase sintering***, enhances the growth of ZnO grains and affects the stability of the nonlinear current–voltage characteristics of the material. The melting point of Bi_2O_3 is 825 °C. The eutectic temperature of ZnO–Bi_2O_3 is only 740 °C, thus a liquid is formed in the ZnO–Bi_2O_3 specimens below 800 °C. As soon as the eutectic liquid is formed, the weight loss starts to increase. This indicates that the vaporization of Bi_2O_3 starts immediately after them eutectic liquid has been formed. Similar to the additives Bi_2O_3, some light metal oxides of transition metal oxides e.g. V, rare earths e.g. Pr and alkaline earths e.g. Ba plays the most important role and segregates to the grain boundary interface [Tsai et al. (1994), (1996)].

In addition to above varistor-former, ZnO varistors consists of several other kinds of additives such as MnO_2, Cr_2O_3, Sb_2O_3 and Co_3O_4, which can be used to enhance non-ohmic properties as well as energy absorption capability and reduces power loss which improve the electrical properties and the stability.

Generally ZnO–Bi_2O_3 and ZnO–Pr_6O_{11} varistor systems cannot be co-fired with a pure silver inner-electrode in multilayered chip varistors because of high sintering temperature (above 1000°C) beyond melting point of silver [Ag mp 961°C]. ZnO–V_2O_5 based ceramics can be well sintered at around 900ºC. This outstanding feature makes ZnO–V_2O_5 based varistor a potential candidate for the fabrication of multi-layered chip varistor using pure Silver as inner electrode instead of the expensive palladium or platinum metals [Tsai et al. (1994), (1996)].

Electrode: At overvoltages the electrical current through the varistor can reach from several hundred up to ten thousand amperes. Therefore electrodes for varistor should satisfy the special requirements. Firstly, electrodes should have a low electric resistance. Secondly, electrodes should not have a transition layer between ceramics and metal, which gives negative effect for current–voltage characteristic of varistor at high electric current. Thirdly, a good coupling between electrode and the surface of ceramics should take place. At present, the silver and aluminum electrodes are used most widely in manufacturing of varistors. Silver electrodes are being created at temperature near 800ºC by means of the silver baking in an air atmosphere. Aluminum electrodes are being created by means of the shooping.

The silver electrodes better satisfy the requirements, which were mentioned above. These electrodes have higher conductive than aluminum electrodes and give a good coupling with the ceramic surface. The copper is also a good electrode material, because of its conductivity is not much lower than the conductivity of silver. However, copper has advantage for varistors production as more cheap material. The compositions of copper-containing pastes for electrodes are known. The annealing process for such pastes demands the neutral or reducing gas atmosphere. However, for varistor ceramics the thermal treatment in such atmosphere is not allowed, because it decreases nonlinearity of current–voltage characteristic.

2.4. ZnO-V_2O_5 based Varistor Ceramics

The ZnO-V_2O_5 system has been mostly studied in glassy material [CaIestani (1986), Sayer (1983)] and it was found that the electrical conduction in the glass was caused by electron hopping between high and low valence ions of the transition metal.

2.4.1. ZnO–V_2O_5 Varistor System

The investigation of the phase diagram of ZnO – V_2O_5 system had a long history since 1965 by many authors [Brown (1965)]. However, the phase diagrams determined differed from each other. The researchers are agreed on the fact that the components of the system under consideration form three compounds: ZnV_2O_6, $Zn_2V_2O_7$and $Zn_3(VO_4)_2$ [Brown (1965), Pollert (1973), Kurzawa (2001)].

On the other hand, Makarov et al. (1971), Clark(1975), and Pick (1975) suggest that, apart from the three vanadates, $Zn_4V_2O_9$ also exists as another compound, which melts incongruently at 910 °C. Vanadate ZnV_2O_6 is not displaying polymorphism [Kurzawa (2001)], which belongs to monoclinic system with space group $C2$. Its lattice parameters are a = 9.2420 Å, b = 3.5260 Å and c = 6.5740 Å. This Vanadate melts incongruently at 645 °C, depositing a high temperature β-$Zn_2V_2O_7$ [Kurzawa (2001)]. $Zn_2V_2O_7$ displays two polymorphs, the temperature of the reversible process; α-$Zn_2V_2O_7$ ↔ β-$Zn_2V_2O_7$ is 620 °C and melts congruently at 890 °C according to Ref. [Makarov et al. (1971)], mean while Clark (1975) and Pick (1975) considered that two temperatures are 615 °C and 872 °C.

Recently, Kurzawa et al (2001) refined the enantiotropic polymorphic process, α-$Zn_2V_2O_7$ ↔ β-$Zn_2V_2O_7$, which takes place at 590±5 °C. $Zn_3V_2O_8$ crystallizes in an orthorhombic system. Its space group is Abam a = 8.2990 Å, b = 11.5284 Å and c = 6.1116 Å. It has been proved that $Zn_3V_2O_8$ did not display polymorphism, but at 800 °C it broke down in a solid phase to yield β-$Zn_2V_2O_7$ and $Zn_4V_2O_9$.

On the other hand, Kurzawa et al. (2001), Makarov et al. (1971) and Clark (1975) and Pick (1975) suggested that there existed another compound $Zn_4V_2O_9$ which melted in congruently at 900 °C or 910 °C. $Zn_4V_2O_9$ was considered to be

metastable by the authors and it crystallizes in a monoclinic system having space group *P*21. Its lattice parameters are *a* = 10.4880 Å, *b*=8.1980 Å, *c* = 9.6820 Å

There are wide divergences of the researchers opinion about polymorphism of zinc orthovanadate (V). Brown (1965) and Hng (1999) point out that $Zn_3(VO_4)_2$ occurs in three polymorphic forms, and the reversible process α-$Zn_3(VO_4)_2$↔β-$Zn_3(VO_4)_2$ takes place at 795 °C. The other reversible polymorphic process, β-$Zn_3(VO_4)_2$↔γ-$Zn_3(VO_4)_2$ runs at 815 °C.

Tsai et al. in 1994, observed non-ohmic behavior for polycrystalline zinc oxide with V_2O_5 as the only additive. The electrical conduction in ZnO-V_2O_5, binary ceramics was a typical schottky barrier controlled current behavior and the nonlinearity characteristics were response to the grain boundary barrier layer. On the basis of the back-to-back Schottky barrier model and thermionic emission theory, an analysis procedure using the I-V and C-V experimental data had been satisfactorily applied to calculate the grain boundary parameters. Taking the ZnO-0.15 mol % V_2O_5 sample as an example, the ***nonlinearity coefficient was 2.8.*** The schottky barrier height was 0.47 eV and the donor concentration N_D was 7.0 x10^{18} cmW^3. From the calculated values of N_D, a transition of defect chemistry from electron compensation to defect compensation was proposed for increase of V_2O_5 doping in ZnO. The sintering behavior of ZnO - V_2O_5 specimens showed that the densification was enhanced and grain growth was promoted in the presence of the V_2O_5 ingredient. Exaggerated grain growth was observed in the specimens containing 0.05 mol % V_2O_5 and above by sintering at 1100 °C for 2 h [Tsai et al. (1994)].

Tsai et al. investigated the microstructure and nonlinear current-voltage characteristics of ZnO - V_2O_5 ceramics sintered at 900 °C. V_2O_5 was the only additive used and the amount ranged from 0.25 to 2 mol%. The isothermal grain growth behavior in zinc oxide ceramics was shown to be strongly influenced by doping with V_2O_5. The results of the microstructural development in ZnO - V_2O_5 ceramics indicate that the grain growth in ZnO ceramics, sintered at 900 °C changed from isotropic growth for pure ZnO to abnormal growth after doping with V_2O_5. The addition of V_2O_5 in ZnO also increased the growth rate of ZnO

grains. This was attributed to the presence of a V_2O_5 rich liquid phase during sintering.

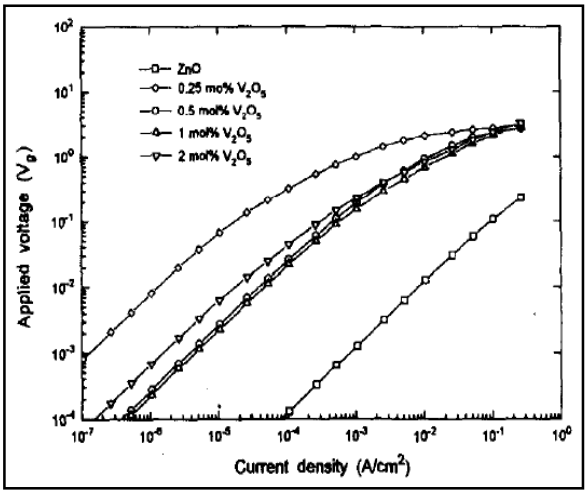

Figure 2.3: The current density versus voltage per grain, V_g,of pure ZnO and ZnO doped with V_2O_5 of 0.25, 0.5, 1 and 2 mol%, respectively. Specimens were sintered at 900°C for 4 h [Tsai et al. (1996)].

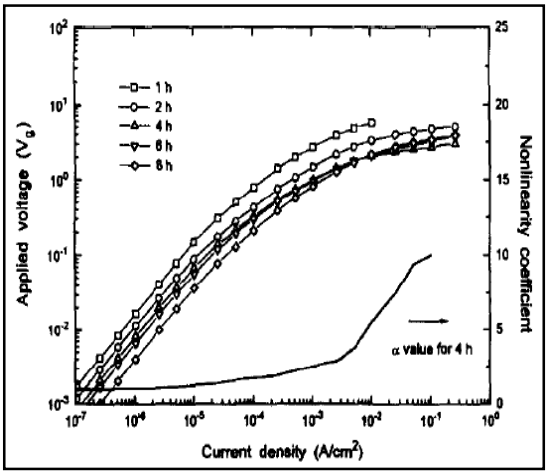

Figure 2.4: Nonlinear *I-V* characteristics of ZnO-0.25 mol% V_2O_5 ceramics sintered at 900°C for various lengths of time. Current density dependence of the nonlinearity coefficient α is a result for the specimen sintered for 4 h [Tsai et al. (1996)].

As shown in Figure 2.3, ***pure ZnO exhibited ohmic behavior and had a resistivity of 4200 Ω cm***. However, the zinc oxide ceramics doped with V_2O_5 exhibited nonohmic behavior. Zinc oxide ceramic doped with 0.25 mol% ***V_2O_5 exhibited nonohmic behavior with α-value comparable to that exhibited by***

binary ZnO-Bi_2O_3, ceramics. It can be seen from the I-V curves shown in Fig. 2.4 that the leakage current increased with increasing sintering time.

However, the increase V_2O_5 content resulted in the reduction of the activation energy (E_a) and the nonlinearity coefficient (α). Sintering time also influenced the I-V properties of the binary ceramics. The exaggerated grains (large), which provide channels of lower resistance between electrodes may play an important role in the electrical properties. Table 2.1 shows the summary of varistor parameters for ZnO-V_2O_5 ceramics sintered at 900°C [Tsai, 1996].

Table 2.1: Summary of Varistor parameters for ZnO-V_2O_5 ceramics sintered at 900 °C.

V_2O_5 (mol %)	Sintering time (h)	Relative density (%)	Average grain size (μm)	Resistivity in ohmic region (MΩ cm)	Onset electric field (V/MM)[a]	Nonlinearity coefficient [b]	Activation energy E_a (eV)
0.00	4	96.9	3.70	0.0042	--	1	-
0.25	4	96.2	10.4	6.31	81	8.9	0.249
0.50	4	95.4	12.6	0.20	14	5.7	0.141
1.00	4	94.0	13.9	0.16	11	3.5	0.130
2.00	4	91.2	12.1	0.55	19	2.8	0.128
0.25	1	96.4	5.40	30.3	508	2.4	0.298
0.25	2	96.7	6.60	16.6	234	3.0	0.272
0.25	6	96.4	19.2	3.40	51	5.0	0.213
0.25	8	96.5	24.3	1.60	34	4.0	0.160

a -> The electric field at 1mA/cm². b -> Measured at V_g = 2.5 V. [Tsai (1996)]

Mirzayi et al. in 2013 investigated the ZnO ceramics with small amounts of V_2O_5 as a varistor-former ranging from 1 – 5 mol% prepared by conventional powder processing route and sintered at 700, 800 and 900 °C for 2 h and it was observed that the grain growth behavior in ZnO ceramics was strongly influenced by doping with V_2O_5. Moreover, lower temperatures about to 900 °C could be used for sintering. They also found that the microstructures of the samples consists of ZnO grains as a main phase and $Zn_3(VO_4)_2$ as a secondary phase. All of the prepared ceramics showed characteristic of non-ohmic current–voltage behavior. Non-linear coefficient increased with increasing in V_2O_5 content and sintering temperature. They also observed that the activation energy of the ceramics lies within the range of 0.071 – 0.402 eV (Table 2.2), which decreased with increase in V_2O_5 content and sintering temperature. The origin of the non-linear electrical behavior was explained by considering the solid state reactions

and formation of the potential barriers at grain boundaries [Mirzayi et al (2013)].

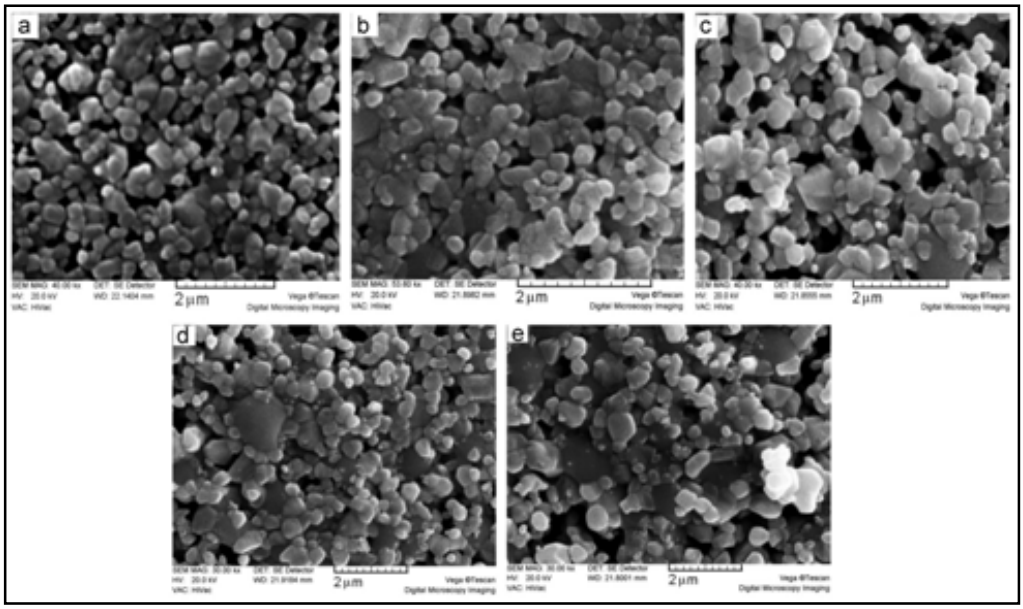

Figure 2.5: SEM micrographs of ceramics sintered at 900 °C containing various amounts of V_2O_5: (a) 1 mol%, (b) 2 mol%, (c) 3 mol%, (d) 4 mol% and (e) 5 mol% [Mirzayi et al. (2013)].

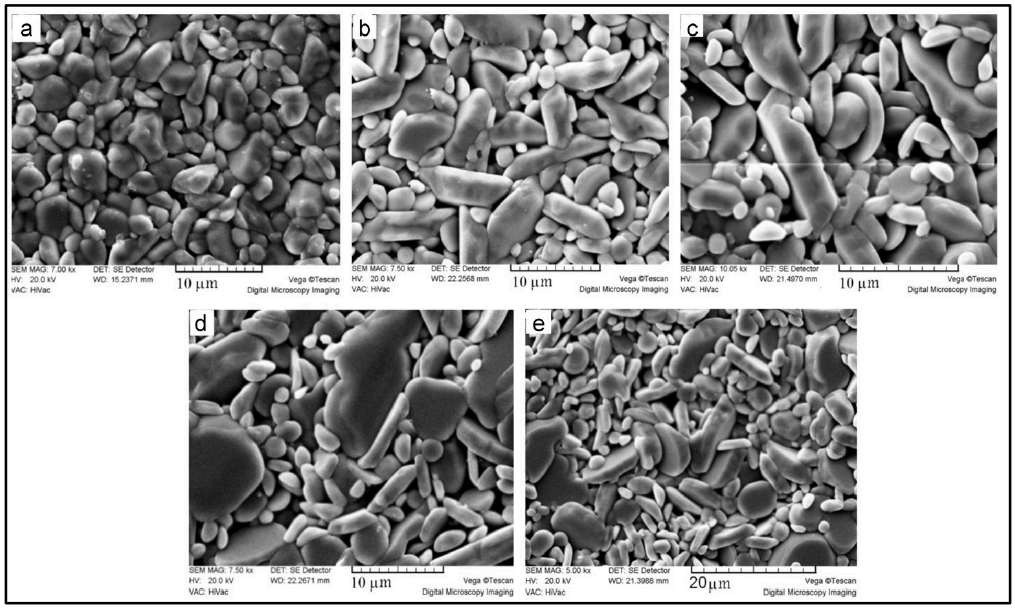

Figure 2.6: SEM micrographs of ceramics sintered at 700 °C containing various amounts of V_2O_5: (a) 1 mol%, (b) 2 mol%, (c) 3 mol%, (d) 4 mol% and (e) 5mol% [Mirzayi et al. (2013)].

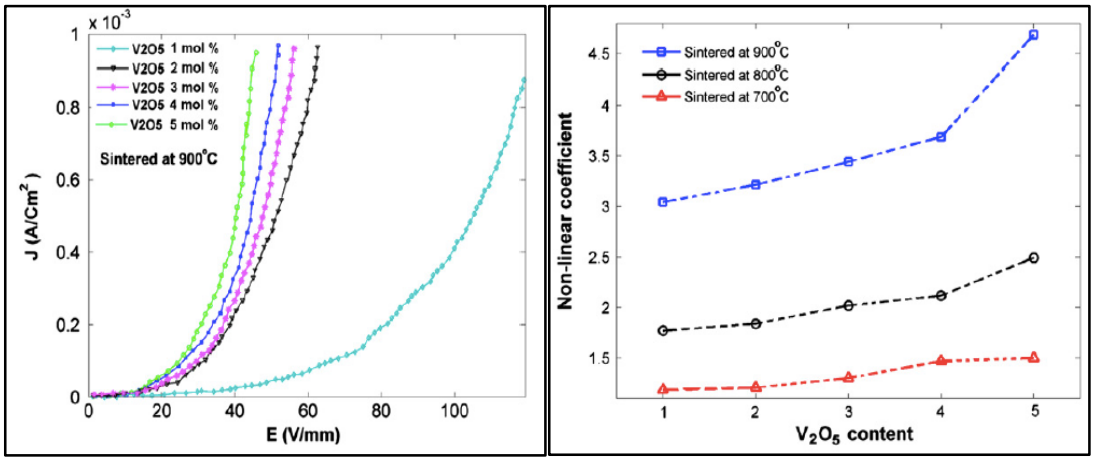

Figure 2.7: Non-linear E–J curve of the prepared ceramics sintered at temperatures 900 ˚C [Mirzayi et al. (2013)]

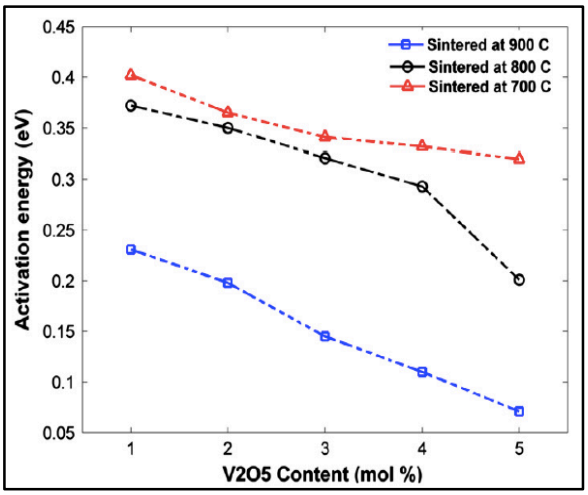

Figure 2.8: Variation of activation energy (E_a) in term of V_2O_5 content and sintering temperature [Mirzayi et al. (2013)]

The abnormal grain growth of ZnO grains was observed in presence of V_2O_5. The grains size increased with increasing V_2O_5 content and sintering temperature. From E–J curves (Figure 2.7), the non-linear coefficient increased with increase in V_2O_5 content and sintering temperature. Activation energy (Fig. 2.8) of the ceramics lies in the range of 0.071–0.402 eV, which decreased with increase in V_2O_5 content and sintering temperature. Table 2.2 shows electrical properties and density of prepared ceramics [M. Mirzayi et al, 2013]. The origin of the non-linear electrical behavior is due to solid-state reactions and formation of potential barriers between grains.

Table 2.2: Electrical properties and density of prepared ceramics

Sintering temperature (°C)	V_2O_5 content (mol%)	Non-linear coefficient	Activation energy (eV)	Density (g/cm³)
900	1	3.053	0.231	5.28
	2	3.220	0.197	5.34
	3	3.437	0.144	5.49
	4	3.689	0.109	5.92
	5	4.702	0.071	6.28
800	1	1.785	0.372	5.10
	2	1.843	0.348	5.26
	3	2.028	0.322	5.60
	4	2.129	0.293	5.70
	5	2.506	0.200	6.01
900	1	1.189	0.402	5.01
	2	1.214	0.366	5.05
	3	1.307	0.342	5.12
	4	1.474	0.333	5.50
	5	1.508	0.320	5.60

[Mirzayi et al. (2013)]

Hng et al. in 2000 studied the effects of the oxide additives i.e. MnO_2, Co_3O_4, and Sb_2O_3, commonly incorporated in commercial Bi_2O_3-doped ZnO varistors, on the current–voltage characteristics and micro-structure of 0.25 mol% V_2O_5 -doped ZnO varistors. The MnO_2 is the most significant additive in terms of its effects on varistor performance. Varistor performance can also be improved by increasing the V_2O_5 content to 0.5 mol% in a ZnO ceramic containing 1 mol% MnO_2. Further increasing the V_2O_5 content of 1 mol% MnO_2 doped material cause deterioration in varistor behavior. The microstructure of the samples consists mainly of ZnO grains with zinc vanadates as the minority secondary phases. Additional spinel phase is formed when Sb_2O_3 is added [Hng et al. (2000)].

Hng et al. (2000) also found that the additions of either MnO_2 or Co_3O_4 did not change the general microstructure of the V_2O_5 doped ZnO varistors that consisted mainly of ZnO grains with a vanadium-rich intergranular layer. The addition of MnO_2 produced the best varistor behavior among the various additives they studied.

Addition of ***Sb_2O_3 to the binary system*** controlled abnormal grain growth and produced a more ***uniform microstructure***, but at the ***expense of a higher sintering temperature***. Low-magnification secondary electron images (SEI)

revealing the typical microstructures of V_2O_5-doped ZnO varistors, which is shown in Fig. 2.9.

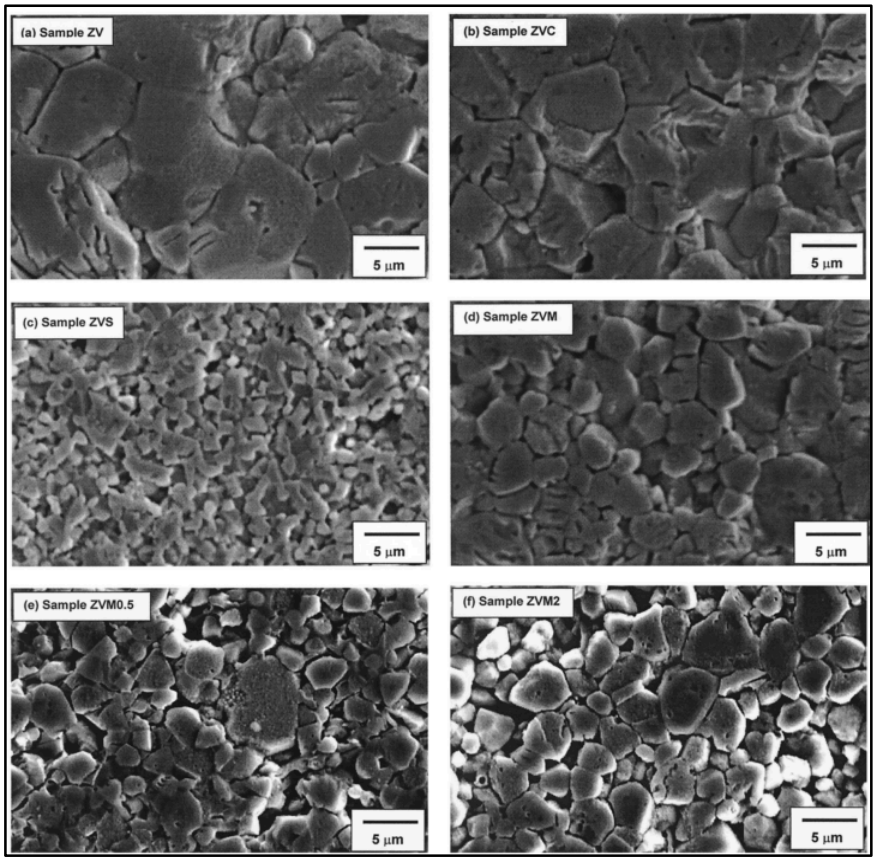

Figure 2.9: SEM micrographs of V_2O_5-doped ZnO varistors [Hng et al. (2000)]

H H Hng et al. also found that a varistor composition of ZnO – 0.5 mol% V_2O_5 –1 mol% MnO_2, in which γ-$Zn_3(VO_4)_2$ was produced at ZnO grain boundaries, produced encouraging I–V characteristics with a low leakage current and a nonlinear coefficient α >18. It is evident that V_2O_5 shows great promise in being able to replace Bi_2O_3 as the varistor forming ingredient in ZnO varistors. Typical *E–J* curves are shown in Fig. 2.10. The lower sintering temperatures that can be used are an especially attractive feature. The low breakdown voltage per grain boundary of ~0.6 V also makes it particularly suitable for the manufacture of low-voltage varistors.

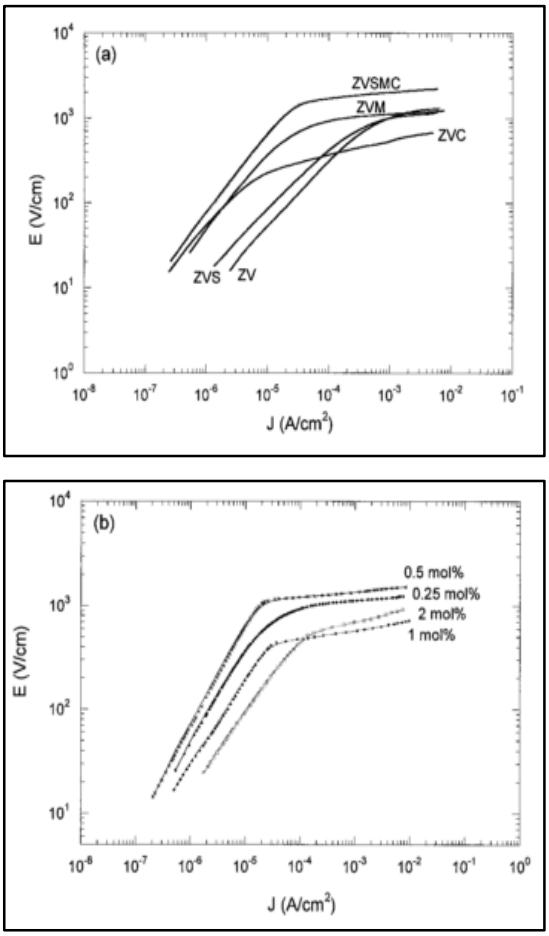

Figure 2.10: *E–J* curves showing (a) effects of additives and (b) effects of V_2O_5 content in Mn doped $ZnO–V_2O_5$ materials [Hng et al. (2000)].

2.4.2. $ZnO–V_2O_5$-Cr_2O_3 Varistor System

Transition metal oxides, such as MnO_2 and Cr_2O_3 additives are generally included to improve the non-ohmic properties of ceramics by increasing the surface-state density, through the formation of interstitial states and deep bulk traps [Greuter (1988)]. They are considered as performance enhancers, in which they improve the non-linearity of the curve and enhance the energy absorption capability of ZnO varistor systems. Although there were numerous studies on the effects of various metal oxides on Bi_2O_3 and Pr_6O_{11} doped ZnO varistors [Greuter (1988), Pianaro (1997), Kim (1995)], such studies on the performance of ZnO–V_2O_5 varistor systems are limited. So, it is required to confirm that whether Cr_2O_3 beneficially affect the ZnO–V_2O_5 system, just as they do for the ZnO – Bi_2O_3 varistor system.

Hng et al. and Chan et al. in 2009 studied the effects of Cr_2O_3 (0.5–4 mol %) on the microstructure and the electrical properties in a binary ZnO–0.5 mol% V_2O_5 system. The microstructure of the samples consists mainly of ZnO grains with $ZnCr_2O_4$ and α-$Zn_3(VO_4)_2$ as the secondary phases. The formation of the $ZnCr_2O_4$ spinel phase (JCPDS 22-1107) is often reported in Bi_2O_3 doped ZnO varistor systems containing Cr_2O_3 [Greuter (1988), Pianaro (1997), Kim (1995)]. This occurs when the amount of added Cr_2O_3 is much higher than the amount of Sb_2O_3 (if present) and when the solubility of Cr_2O_3 in Bi_2O_3 is exceeded. The addition of Cr_2O_3 is found to be effective in controlling the abnormal ZnO grain growth often found in V_2O_5 doped ZnO ceramic system, and more uniform microstructure obtained. The varistor performance is also improved as observed from the increase in the non-linear coefficient (α) of the Cr_2O_3-doped ZnO–V_2O_5 samples. The 'α' value is found to increase with the increase of Cr_2O_3 up to 3 mol% Cr_2O_3 content. Further increase in Cr_2O_3 is found to cause a decrease in α value. The highest α value reported by Hng was obtained for the ZnO – 0.5 mol% V_2O_5 – 3 mol% Cr_2O_3 sample.

2.5. Impedance Spectroscopy Studies of Grain Boundary Phenomena in the Zinc Oxide based Varistors

The electrical performances of ZnO varistors critically depends on the microstructure characteristics where the ***electrical characteristics can be controlled by modifying the microstructure at the grain boundary***. The nonlinear characteristics are attributed to the formation of double schottky barriers (DSB) at the ZnO grain boundaries. Therefore, there have been numerous studies addressing the grain boundary phenomena of ZnO-Bi_2O_3 [Pandey (2007), West (1997), Chen (2015)] and ZnO-V_2O_5 based ceramics systems [Ting (2011), (2012)]. It is vital to the comprehension of the mechanism controlling the grain boundary processes of ZnO varistor based ceramics. It may also enable a researcher or manufacturer to tailor the grain boundary behavior of ZnO based varistor ceramics in a more efficient way according to the specific demands of application. The grain boundary behavior can be profoundly affected by the dopants.

Chen et al. (2015) found that the values of the breakdown field E_{1mA} and nonlinear coefficient are strongly dependent on the resistivity of the grain boundary.

Wu et al. (1996) studied the influence of MnO_2, PbO and a mixture of MnO_2, PbO, and B_2O_3 on the electrical and dielectric properties of ZnO - V_2O_5 ceramics by alternating-current (AC) impedance and variable-temperature dielectric spectroscopy and they found that the schottky barrier present at the grain boundary is much more important for varistor performance.

Tsai et al. (1994) found that there are no Debye relaxation peaks at room temperature for the ZnO - V_2O_5 based ceramics. Nahm et al. (2007, 2011 and 2015) revealed that a weak dielectric dispersion peak appeared in the ZnO -V_2O_5 - Mn_3O_4 and ZnO - V_2O_5 - MnO_2 systems.

AC impedance spectroscopic analysis of doped and un-doped $ZnO–V_2O_5$ based varistor ceramics:

Wu et al (2012) studied ZnO-V_2O_5 (ZV), ZnO-V_2O_5-MnO_2 (ZVM), ZnO-V_2O_5-PbO (ZVP) and ZnO-V_2O_5-MnO_2-PbO-B_2O_3 (ZVMP) ceramics by alternating-current (AC) impedance and variable-temperature dielectric spectroscopy. They found that, compared with the resistivity of the intervening layer at the grain boundary, the schottky barrier present at the grain boundary is much more important for varistor performance, which can be significantly improved by using a mixture of MnO_2, PbO, and B_2O_3.

Consequently, better varistor performance is achieved for 94.5 mol.% ZnO + 0.5 mol.% V_2O_5 + 1.0 mol.% MnO_2 + 2.0 mol.% PbO + 2.0 mol.% B_2O_3 (ZVMPB), i.e., nonlinear coefficient (α) = 35.3 and leakage current density (I_L) = 2.72 $\mu A/cm^2$. SEM images of different specimens are shown in Fig. 2.11. E–J curves of different specimens tested at room temperature are shown in Fig. 2.12 [Wu et al (2012)].

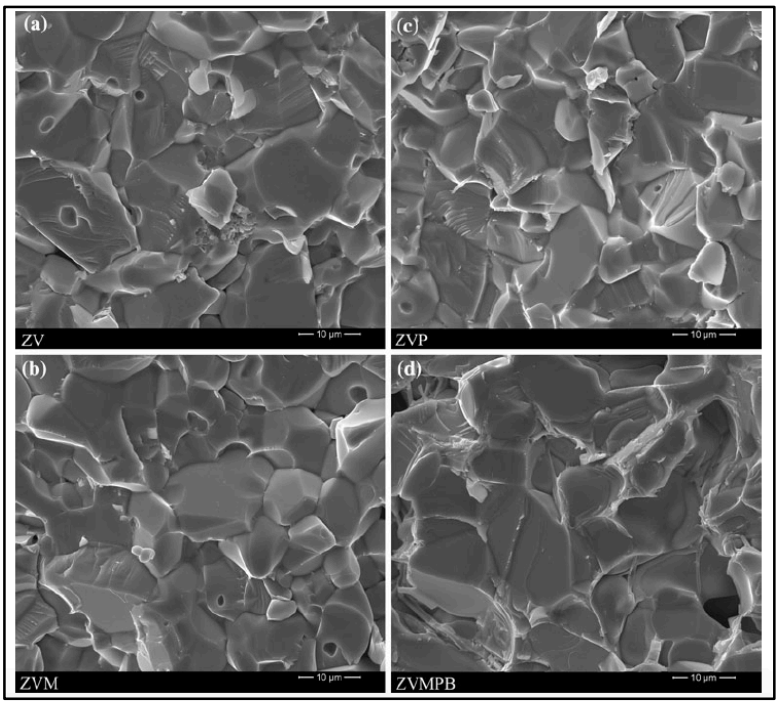

Figure 2.11: SEM images of different specimens: (a) ZV, (b) ZVM, (c) ZVP, and (d) ZVMPB [Wu et al (2012)].

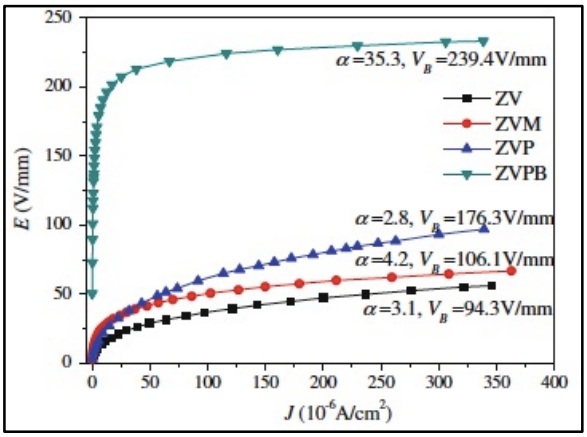

Figure 2.12: E–J curves of different specimens tested at room temperature [Wu et al (2012)]

Wu et al (2012) reported that:

a) The resistivity of the grain boundaries and Schottky barrier height φ_B can be significantly increased by addition of MnO_2, especially by a mixture of MnO_2, PbO, and B_2O_3.

b) PbO dopant increases the resistivity of grain boundaries; it simultaneously decreases the Schottky barrier height φ_B, thus decreasing the electrical properties of ZVP.

These results indicate that the Schottky barrier height at grain boundaries is much more important than the resistivity of the intervening layer at the grain boundaries for the varistor performance. The results of variable-temperature dielectric spectroscopy show that an effective depletion layer formed in all of the specimens. The activation energy of the characteristic dielectric relaxation process in the depletion layer is found within the range of 0.339 eV to 0.365 eV, indicating that this dielectric relaxation process is associated with oxygen vacancy V_O [Wu et al (2012)].

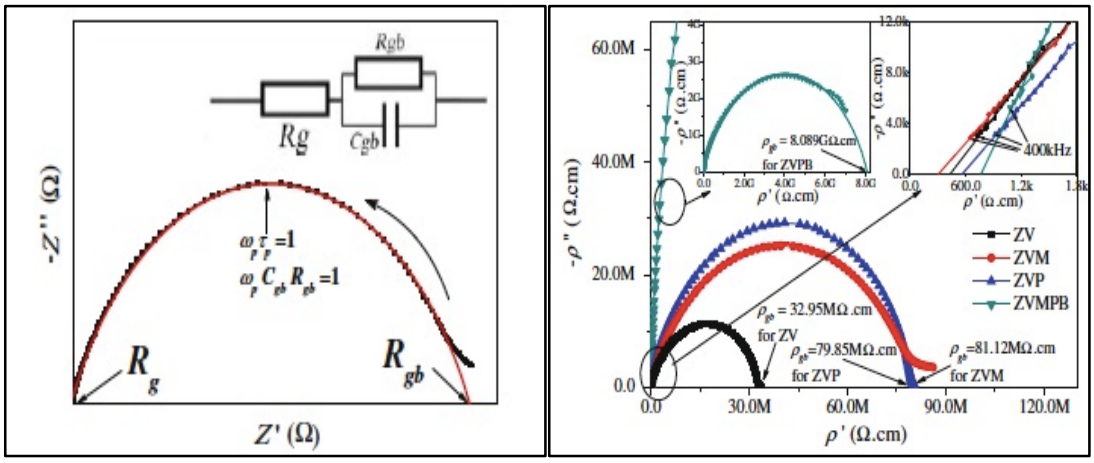

Figure 2.13: (a) A typical equivalent circuit, a sketch of the AC impedance spectrum and (b) AC impedance spectra of the specimens tested at room temperature [Wu et al (2012)].

They used most common and accepted one equivalent circuit models used by Wu et al (2012) in their research work. It is shown in the inset in the upper-right corner of Figure 2.13(a), which is use to identify the characteristics of the grain and grain boundary in ZnO-based varistors. Where R_g represents the equivalent resistance of the grains, and R_{gb} and C_{gb} represent the equivalent resistance and capacitance of the grain boundaries, respectively. The values of R_g, R_{gb}, and C_{gb} can be derived from the AC impedance spectrum, the real part of which can be expressed as [Wu et al (2012)]

$$Z'_{(\omega)} = R_g + \frac{R_{gb}}{1 + (\omega C_{gb} R_{gb})^2},$$

where ω is the angular frequency (x = 2πf, where f is the frequency). Thus, it can be deduced that $Z'(0) \approx R_g + R_{gb}$ as $\omega \rightarrow 0$ (low frequency) and $Z'(\infty) \approx R_g$ as $\omega \rightarrow \infty$ (high frequency). Since $R_{gb} >> Rg$, $Z'(0) \approx R_{gb}$. Therefore, the values of Z'(0) and Z'(∞), i.e., R_{gb} and R_g, may be estimated from the intercept on the real axis (Z') of the corresponding semicircle fitted to the AC impedance spectrum in the high- and low-frequency regions, respectively, as shown in Fig. 2.13(b). In this work, the data were normalized to the electrode area A and the sample thickness (t), i.e., ρ' = Z'A/t and ρ"= Z"A/t, where ρ' and Z' are the real parts and ρ" and Z" are

the corresponding imaginary parts of the resistivity and the AC impedance respectively.

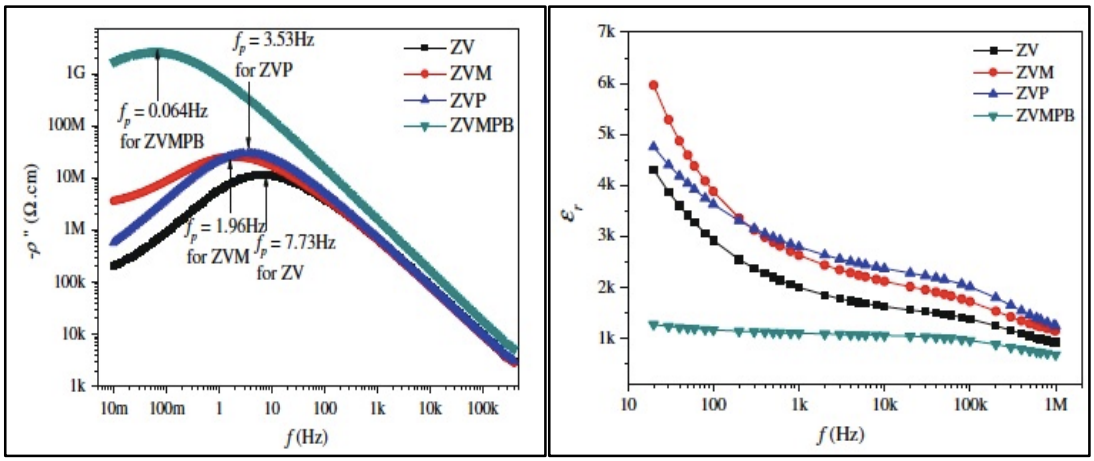

Figure 2.14: Frequency dependence of – ρ" of different specimens and Frequency dependence of the relative dielectric constant of the specimens tested at room temperature [Wu et al (2012)].

Another work done by Wu et al (2012), the electrical and dielectric properties of MnO_2 doped and un-doped ZnO – V_2O_5 ceramics were studied by AC impedance and variable temperature dielectric spectroscopy.

The results show that V and Mn ions simultaneously segregated at the grain boundaries to form an intergranular phase, which increases the resistivity of the intervening layer and the Schottky barrier at the grain boundaries, and then improving the varistor performance. An obvious loss peak appeared in all the samples, which means an effective depletion layer has formed. As for the samples sintered at 1,000°C for 2 h, the activation energy of the characteristic relaxation process is about to 0.339 eV for 99.5 mol% ZnO + 0.5 mol% V_2O_5 (ZV) and 0.352 eV for 99.0 mol% ZnO + 0.5 mol% V_2O_5 + 0.5 mol% MnO_2 (ZVM) respectively, which indicate that this relaxation process is associated with oxygen vacancy V_O.

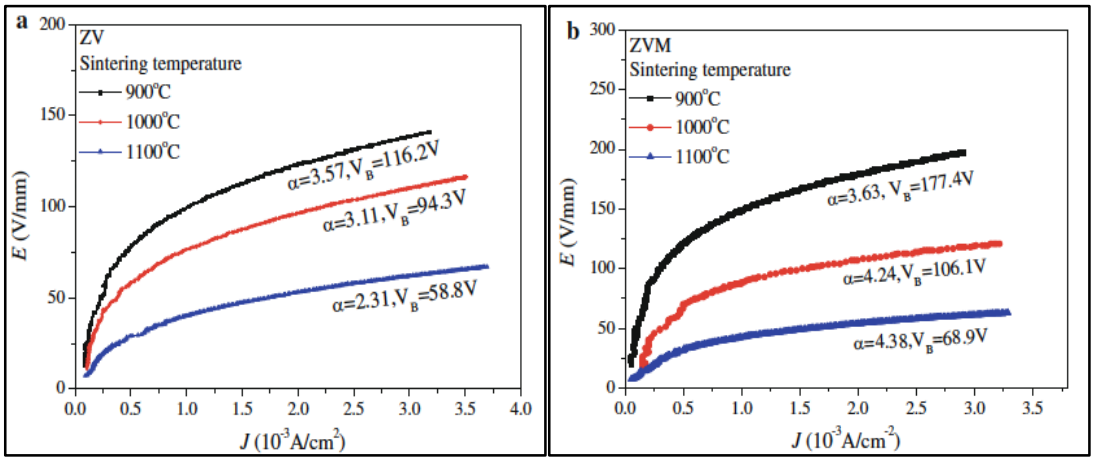

Figure 2.15: J–E curves of the samples sintered at different temperatures (a) ZV and (b) ZVM [Wu et al (2012)]

Jun Wu et al (2012) investigated that, not only the resistivity of the intervening layer but also the schottky barrier height φ_B at the grain boundaries can be increased significantly by the addition of MnO_2 at the sintering temperature ranging from 900 – 1100 °C.

As for the samples sintered at 1,000°C for 2 h, the electronic defect states are obviously increased by the MnO_2 dopant and then the schottky barrier height (φ_B) increases from 0.285 to 0.351 eV.

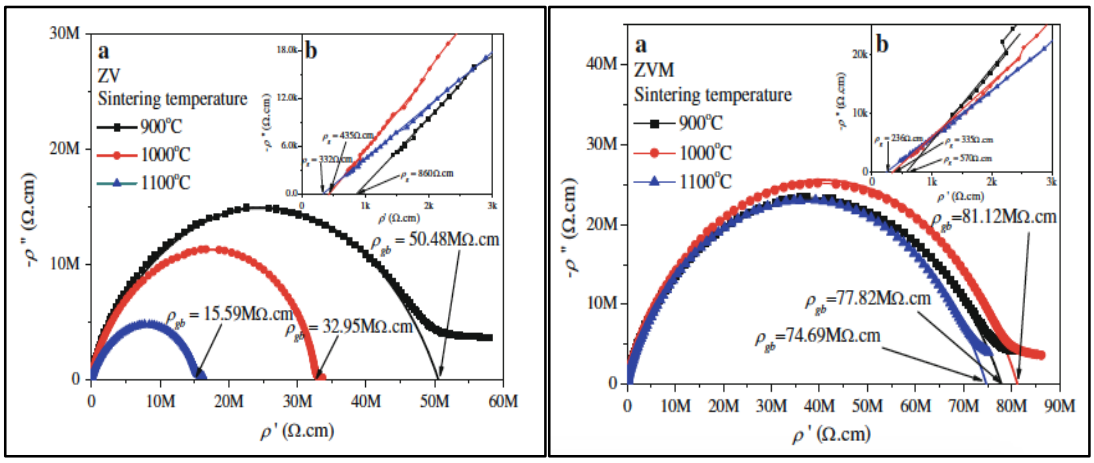

Figure 2.16: Ac impedance spectra of a) ZV& b) ZVM sintered at different temperatures [Wu et al (2012)].

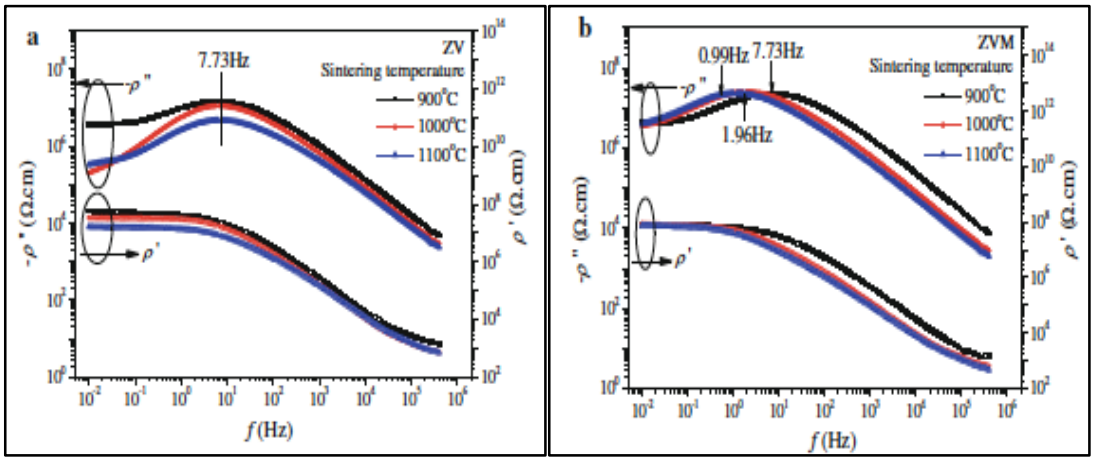

Figure 2.17: Frequency dependence of-ρ' and –ρ" of a ZV and b ZVM [Wu et al (2012)]

A loss peak appears in all the samples were reported by Wu et al (2012), which means an effective depletion layer has formed. The frequency of the characteristic relaxation peak f_m at room temperature is 600 kHz for 99.5 mol% ZnO + 0.5 mol% V_2O_5 and at 300 kHz for 99.0 mol% ZnO + 0.5 mol% V_2O_5 + 0.5 mol% MnO_2, respectively. The activation energy of the characteristic relaxation process is about to 0.339 and 0.352 eV for ZnO-V_2O_5 (ZV) and ZnO-V_2O_5-MnO_2 (ZVM) sintered at 1000°C for 2 h respectively, which means it is associated with oxygen vacancy V_O.